IEEE Access
Multidisciplinary | Rapid Review | Open Access Journal

Received February 9, 2020, accepted February 26, 2020, date of publication March 2, 2020, date of current version March 12, 2020.

*Digital Object Identifier 10.1109/ACCESS.2020.2977616*

# Broadband Antenna Design With Integrated CB-CPW and Parasitic Patch Structure for WLAN, RFID, Wimax, and 5G Applications

**ZHENDONG DING, DAN ZHANG, (Member, IEEE), AND CHUNYU MA**
College of Information Science and Technology, Nanjing Forestry University, Nanjing 210037, China

Corresponding author: Dan Zhang (zhangdan@njfu.edu.cn)

This work was supported in part by the National Natural Science Foundation of China and High-Level Talents Program of Nanjing Forestry University under Grant 31170668 and Grant 163070694.

**ABSTRACT** This paper presents a novel CB-CPW wideband antenna design. HFSS software simulations reveal that the proposed design has a semicircle ground structure, transmission line, parasitic ground, CPW, relatively low return loss, broadband effect of 3.3377 GHz (4.8337 GHz-8.1714 GHz), double beam capability at 5.2 GHz, and four-beam capability at 5.5 GHz (5.8 GHz). It is compact in size at only 40 mm×40 mm ×1 mm. A prototype of the proposed antenna was fabricated and measured to validate the simulated design; the results show a bandwidth of 3.38 GHz (3.95 GHz-7.33 GHz), relative bandwidth of 74%, and maximum gain of 3.87 dBi in the range of 5 GHz to 6 GHz; the prototype also achieves two and four-beam performance. Its working frequency covers WLAN (5.15 GHz-5.25 GHz and 5.725 GHz-5.825 GHz), radio frequency identification RFID (5.8 GHz), and global microwave internet access WiMAX (5.25 GHz-5.85 GHz) frequency bands.

**INDEX TERMS** Microstrip antenna, parasitic ground, CB-CPW, bandwidth, gain.

## I. INTRODUCTION

Modern wireless communication systems [1] require multi-function, high-speed, small-size, high-performance communication equipment. The performance of traditional communication equipment in today's communications field does not satisfy the requirements of 5G wireless systems [2], [3]. Newer 5G antennas [6]–[8] are designed for multi-adaptation, multi-function, and multi-demand characteristics. Similarly, the fields of Big Data [1] and LiDAR [4], [5] also need the receiving and transmitting functions of new antennas. Reducing the antenna's size is also a hot topic in the communication equipment research field.

Among them, microstrip antenna is a thin dielectric substrate, one side of which is attached with a thin metal layer as the grounding plate, and the other side is made into a certain shape of metal patch by photography. However, simply shrinking the antenna can affect its standing-wave, gain, bandwidth, and other index characteristics. It is a challenging task to reduce the size of the antenna properly without sacrificing its performance. The antenna may instead be optimized using such structures as the coplanar waveguide (CPW) [9]–[12].

There are currently several wireless band standards such as IEEE 802.16 [13], [14], the Worldwide Interoperability for Microwave Access (WiMAX) system around 2.5-2.69/3.4-3.69/5.25-5.85 GHz, and IEEE 802.11a [15], [16], the Wireless Local Area Network (WLAN) in the frequency band of 5.15-5.25 and 5.725-5.825 GHz, which are widely applied in wireless communication systems.

The CPW has many advantages. It can be integrated with other microwave devices for miniaturization while retaining the integrity of the circuit. The dispersive property of CPW transmissibility is better than that of the microstrip line; it can realize broadband effects in the circuit and antenna. The CPW can also transmit odd and even modes, which makes the antenna design highly flexible. CPW designs have garnered a great deal of research interest to this effect.

Previous researchers have indeed developed a number of CPW structures. These include special slot antennas fed by the CPW structure, such as the stair-shaped slot [17] and regular-hexagonal slot [18]. Other scholars have developed a dual-band and dual-sense circularly polarized CPW-fed monopole antenna with two rectangular parasitic elements

The associate editor coordinating the review of this manuscript and approving it for publication was Guan Gui.

**TABLE 1. Comparison Of proposed antenna with other reported antennas.**

| Ref. number | Size($mm^3$) | Operating band (GHz) |
|---|---|---|
| [16] | 60×40×0.8 | 2.3-3.15 |
| [17] | 62×62×3 | 1.8-4.5 |
| [18] | 63×75×1.6 | 1.81-3.83 |
| [19] | 100×120×0.762 | 1.73-3.11 |
| [20] | 70×70×1.6 | 1.5-2.5 |
| [21] | 50×50×1 | 1.71-3.66 |
| [22] | 30×20×1.6 | 2.33-3.56 |
| [6] | 60×60×0.8 | 2.67-13 |
| [23] | 48×42×2 | 3-13 |
| Proposed | 40×40×1 | 4.8337-8.1714 |

and an I-shape grounded stub [19]. Some devices have relatively large size and relatively small bandwidth [17]–[19]. An antenna with a compact and broadband CPW-fed meander-slot structure [6] is effectively miniaturized but its bandwidth is only 2.33-3.56 GHz. By contract, an antenna that is ideal for broadband is relatively large in size [23]. Other broadband-capable, small-size antennas have been proposed as well [24]. The bandwidth and size of some representative devices are listed in Table 1.

This paper proposes a conductor-backed (CB-CPW) broadband antenna with multi-beam performance for WLAN, RFID, and WiMAX applications. The proposed device has a semi-circular grounding structure, parasitic grounding, and three CPW structures that achieve its broadband effect. It readily dissipates heat and has high mechanical strength; it also is compact in size and has a simple, straightforward configuration. A prototype of the antenna shows satisfactory performance, as discussed in detail below.

Table 1 shows a comparison of the size and broadband effect of the proposed antenna and various other antenna designs. Each has advantages and disadvantages. The proposed antenna was designed and optimized on the basis of such advantages. It can realize radiation in double-beam and four-beam directions, among other advantageous performance characteristics as discussed in greater detail below.

## II. ANTENNA ANALYSIS AND DESIGN

### A. THEORETICAL ANALYSIS

The coplanar waveguide structure is composed of two grounding planes on the same side of the transmission line and the transmission line on the dielectric substrate, as shown in Fig. 1(a). The fed planar antenna system mainly

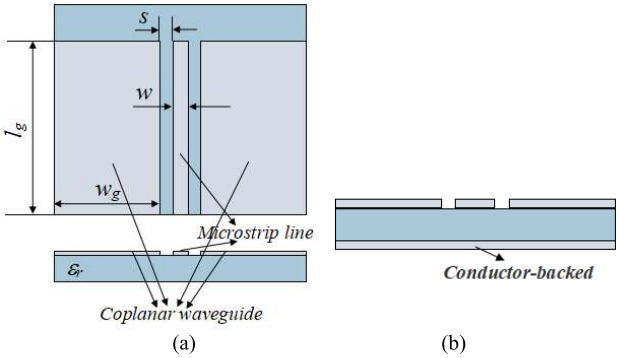


**FIGURE 1. (a) Traditional CPW and (b) CB-CPW.**

includes a broadband antenna, circular polarization antenna, multi-mode antenna, and other equipment related to the CPW structure; among them, the broadband antenna is the most commonly used. Its primary mode is TEM. The CB-CPW structure, as shown in Fig. 1(b), presents the favorable transmission performance of CPW as well as easy heat dissipation and high mechanical strength characteristics.

The CB-CPW structure is mainly capable of producing resonance phenomena. Under cavity model theory, the ground plane at both ends and the back plane can be regarded as two patch resonators which are surrounded by ideal magnetic walls. Throughout the structure, the signal in the middle passes through the gap of S on both sides as coupling electromagnetic energy is provided to the two resonant cavities. This generates a resonant frequency. Under transmission line theory, the ratio of wave voltage to current on the transmission line can be defined as the characteristic impedance of the transmission line, namely $Z_0$. The input impedance is $Z_{in}$.

The resonant frequency [25] and the impedance of the CPW structure can be calculated as follows:

$$f_{mn} = \frac{c}{2\sqrt{\varepsilon_r}}\left[\left(m/w_g\right)^2 + \left(n/l_g\right)^2\right]^{0.5} \quad (1)$$

$$Z_0 = \sqrt{L/C} \quad (2)$$

where $f_{mn}$ is the resonant frequency, $Z_0$ is the impedance, $c$ is the speed of light, $\varepsilon_r$ is the relative permittivity of the material, $m$ and $n$ are factors of the resonant mode, $w_g$ and $l_g$ are the width and length of the ground plane at both ends of CPW, respectively, and $L$ and $C$ are the distributed capacitance and distributed inductance of the transmission line, respectively.

The simplified network mode of the microstrip antenna was also analyzed for the purposes of this study as shown in Fig. 2.

Based on the equivalent circuit (Fig. 2) and the approximation of $L' \approx 0$, the input impedance reduces to:

$$Z_{in} \approx \frac{1}{1/R_{mn} + j[\omega C_{mn} - 1/(\omega L_{mn})]} \quad (3)$$

where $Z_{in}$ is the input impedance for the $TM_{mn}$ mode and $R_{mn} = 1/G_{mn}$. At resonance, $Q$ is given by Eq. (4)

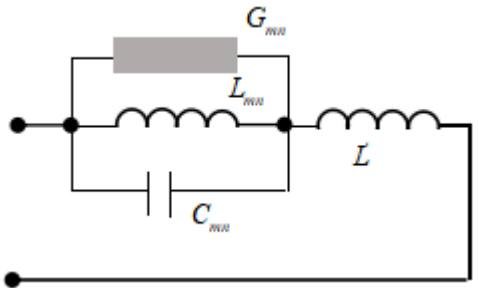


**FIGURE 2.** Simplified network mode (valid when $\omega$ *mn* is well-separated from all other resonant frequencies).

and $\omega_{mn} = 1/\sqrt{L_{mn}C_{mn}}$.

$$Q = 2\omega_{mn}\left(\frac{C_{mn}V^2/2}{V^2/R_{mn}}\right) = \frac{R_{mn}}{\sqrt{L_{mn}/C_{mn}}} \tag{4}$$

Thus, Eq. (3) may be rewritten as:

$$Z_{in} = \frac{1}{1 + jQ[f/f_{mn} - f_{mn}/f]} = \frac{R_{mn}}{1 + jQS} \tag{5}$$

Assuming that the characteristic impedance of the feed line equals to $R_{mn}$, then the norm of the reflection coefficient $|\Gamma|$ is:

$$|\Gamma| = \left|\frac{Z_{in} - R_{mn}}{Z_{in} + R_{mn}}\right| = \left[1 + \frac{4}{Q^2S^2}\right]^{-1/2} \tag{6}$$

Consequently,

$$\frac{\rho + 1}{\rho + 1} = \frac{1}{|\Gamma|} = \left[1 + \frac{4}{Q^2S^2}\right]^{1/2} \tag{7}$$

and

$$S = \frac{f}{f_{mn}} - \frac{f_{mn}}{f} = \pm\frac{\rho - 1}{Q\sqrt{\rho}} \tag{8}$$

where $\rho$ is the Voltage Standing Wave Ratio (VSWR).

In Eq. (8), the minus sign represents the lower frequency $f_L$ and the plus sign the higher one $f_H$. As per Eq. (8), both $f_L$ and $f_H$ can be resolved to ultimately express the relative bandwidth (BW) as follows:

$$BW = \frac{f_H - f_L}{f_{mn}} \times 100\% = \frac{\rho - 1}{Q\sqrt{\rho}} \times 100\% \tag{9}$$

$$P_r = \frac{1}{2}\sqrt{\frac{\varepsilon}{\mu}}\frac{V^2}{\pi}\int_0^{\pi}\frac{\sin^2(ka\cos\theta/2)}{\cos^2\theta}\sin^3\theta d\theta \tag{10}$$

$$G_r = \frac{2P_r}{V^2} \tag{11}$$

$$G_s = 1/2G_r = S/120\pi^2 \tag{12}$$

The directivity $D_0$ can be obtained from Eqs. (10)-(12). The maximum radiation is at $\theta = \varphi = 90°$ and

$$D_0 = \frac{|E_{\max}|^2 r^2}{60P_r} = \frac{2}{15G_r}\left(\frac{a}{\lambda}\right)^2 = \frac{1}{15G_s}\left(\frac{a}{\lambda}\right)^2 \tag{13}$$

where *Emax* is the maximum electric field strength, a = w is the radiation edge, and $\lambda$ is the wavelength in free space.

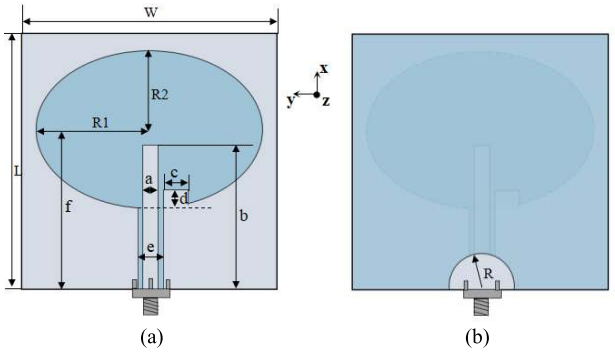


**FIGURE 3.** Geometry of proposed antenna: (a) front side and (b) back side, where L=W=40 mm, R1=12 mm, R2=18 mm, H=1 mm, R=4.5 mm, a=2 mm, b=20 mm, c=4.5 mm, d=1.4 mm, e=2.4 mm, f=24 mm.

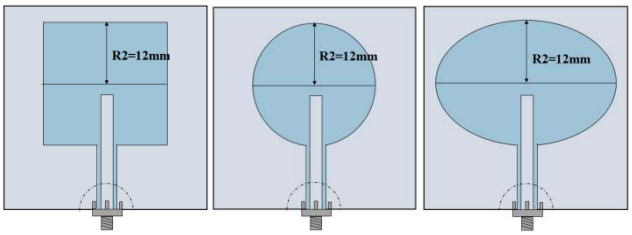


**FIGURE 4.** Comparison of three antenna geometric shapes. (a) Antenna 1, (b) Antenna 2 and (c) Antenna 3 respectively correspond to the square, circle and ellipse to be cut off.

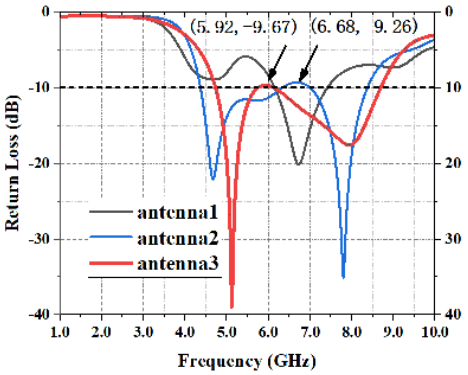


**FIGURE 5.** Return loss comparison of three antenna shapes.

### *B. ANTENNA DESIGN*

The antenna proposed in this paper is based on a CB-CPW with a rectangular parasitic patch, transmission line and back semi-circular grounding structure. It is similar to a previously published CB-CPW design [25] and differs from the traditional CB-CPW due to its parasitic patch. The a back ground of the antenna in this paper is a small semicircle structure. Some references [26], [27] also have some small a back ground. The proposed antenna design is illustrated in Fig. 3.

The antenna structure is composed of a dielectric base unit, a transmission line unit, a back ground, and a coplanar ground. The material of the dielectric base unit is FR4 with a relative dielectric constant of 4.4, and the size is L× W×H. Other unit materials are all metallic copper. Their specific dimensions and values are also shown in Fig. 3.

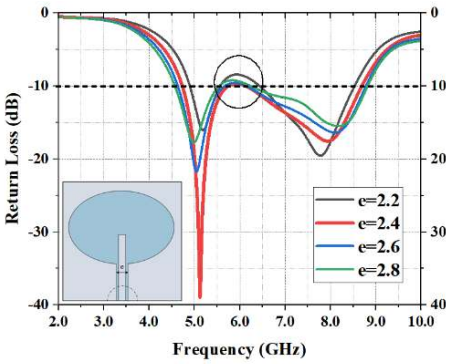


(a)

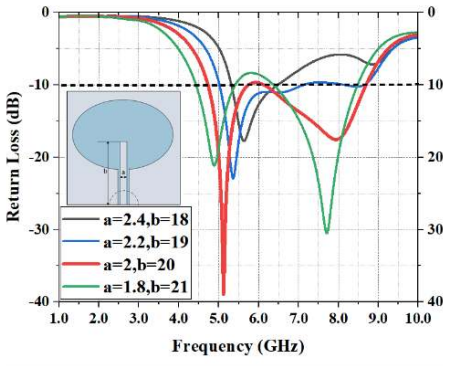


(b)

**FIGURE 6.** Size optimization (a) e parameter optimization for S11 and (b) a and b parameter optimization of S11.

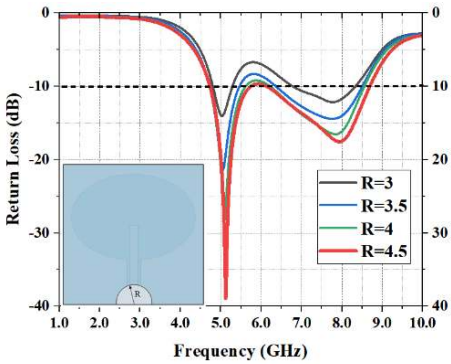


(a)

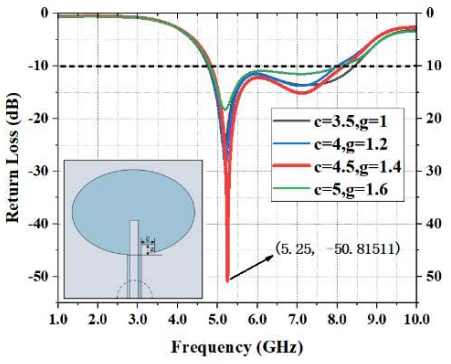


(b)

**FIGURE 7.** Size optimization (a) R parameter optimization for S11 and (b) c and g parameter optimization of S11.

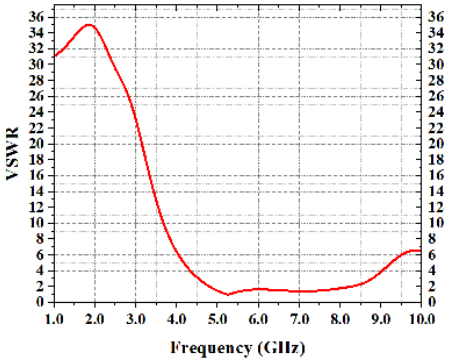


**FIGURE 8.** Microstrip antenna simulation VSWR.

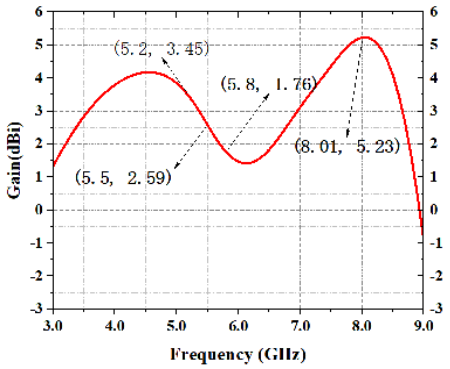


**FIGURE 9.** Microstrip antenna simulation gain.

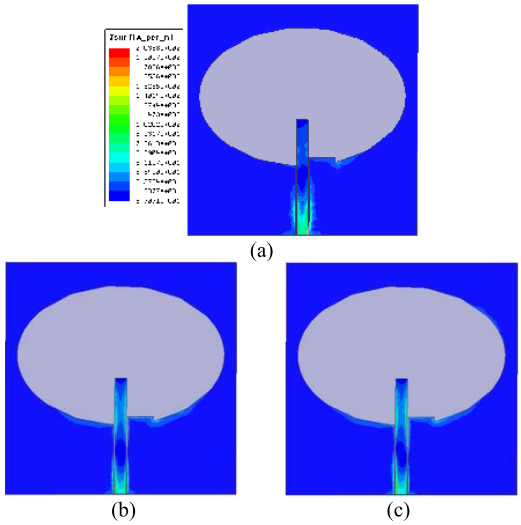

(a) (b) (c)

**FIGURE 10.** Simulated surface current distributions for proposed antenna at (a) 5.2 GHz, (b) 5.5 GHz, (c) 5.8 GHz.

As shown in Fig. 4, Antenna 1 is a square cut off from the common surface, Antenna 2 is a circle cut off from the common surface, Antenna 3 is an ellipse cut off from the common surface; in the three structures, R2=12 mm. As shown in Fig. 5, Antenna 3 has the best effect; but its return loss cannot be less than −10 dB at 5.9 GHz, so it yet merits optimization for further improvement.

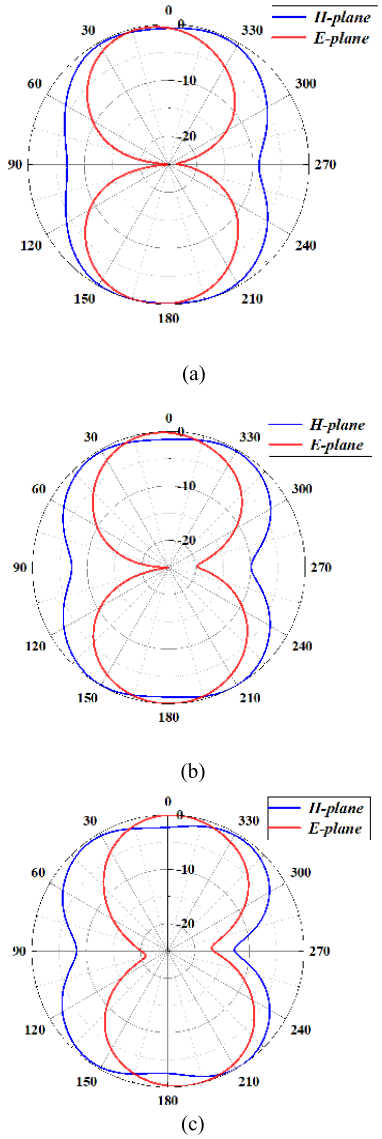


**FIGURE 11.** Simulated 2-D radiation pattern (E-plane and H-plane) at (a) 5.2 GHz, (b) 5.5 GHz, (c) 5.8 GHz.

As shown in Fig. 6(a), the influence on return loss was observed in this study by adjusting the size of the gap on both sides of the transmission line and taking four sizes, e=2.2 mm, e=2.4 mm, e=2.6 mm, and e=2.8 mm, respectively. The effect is best when e=2.4 mm, but the return loss in this case is still higher than −10dB. As shown in Fig. 6(b), the length and width of the transmission line were adjusted to select four displays, a=2.4 mm and b=18 mm, a=2.2 mm and b=19 mm, a=2 mm and b=20 mm, and a=1.8 mm and b=21 mm, respectively. The effect is best when a=2 mm and b=20 mm, and the return loss is higher than −10 dB.

As shown in Fig. 7(a), the size of the back ground patch was adjusted next and radii R=3 mm, R=3.5 mm, R=4 mm, and R=4.5 mm were respectively tested. The effect is best when R=4.5 mm and the return loss is just below −10 dB. The antenna was designed for expanded bandwidth. Joining the parasitic patch can expand the bandwidth,

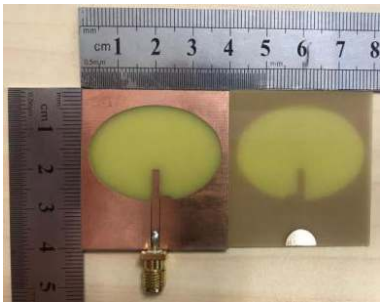

**FIGURE 12.** Front and back of antenna prototype.

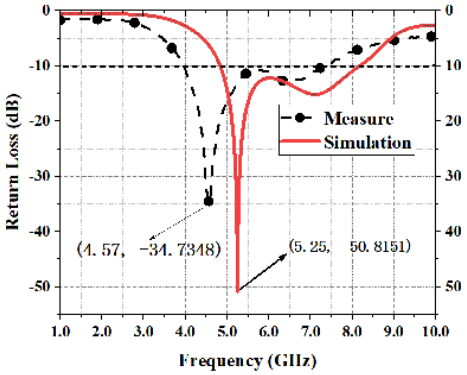


**FIGURE 13.** Simulation and measurement data of proposed antenna return loss.

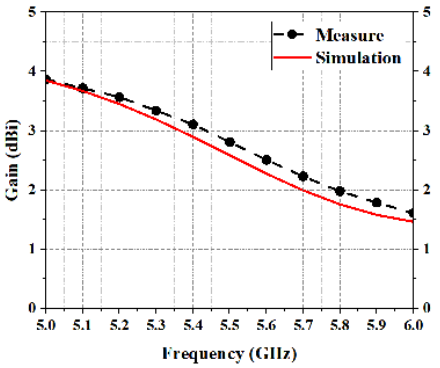


**FIGURE 14.** Simulation and measurement data of proposed antenna gain(5GHz to 6GHz).

so a parasitic square patch antenna was added to the CPW structure (Fig. 7(b)) with length and width of c = 3.5 mm and g = 1 mm, c = 4 mm and g = 1.2 mm, c = 4.5 mm and g = 1.4 mm, and c = 5 mm and g = 1.6 mm, respectively. As shown in Fig. 7(b), the bandwidth is broad with favorable return loss when c = 1.4 mm and g = 4.5 mm.

According to the simulation results, the antenna achieves resonance at the frequency $f$ = 5.25 GHz and return loss S11= −50.81511 dB at the optimal resonance point. When S11= −10dB, $f_L$ = 4.8337 GHz and $f_H$ = 8.1714 GHz. Between $f_H$ and $f_L$, S11 < −10 dB. The absolute bandwidth of the antenna B = $f_H$-$f_L$ = 3.3377 GHz and the relative bandwidth Br = 64%.

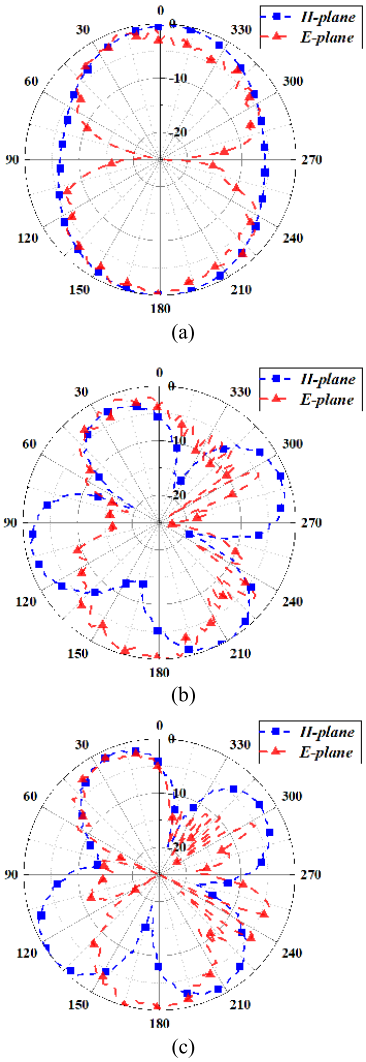


**FIGURE 15.** Measured 2-D radiation pattern (E-plane and H-plane) at (a) 5.2 GHz, (b) 5.5 GHz, (c) 5.8 GHz.

### C. SIMULATION INDEX

The shape and size of the proposed antenna were optimized as discussed above. Other parameters of the antenna were also simulated as discussed in this section. HFSS software was to test parameter performance. Return loss and standing wave are one index which can be converted into each other. As shown in Fig. 8, VSWR is generally required to be less than 2 or 2.5 in engineering practice. The VSWR (Fig. 8) is all less than 2 in the bandwidth, indicating effective VSWR performance in the proposed design.

The relationship between simulation gain and frequency is shown in Fig. 9. The gain of 5.2 GHz, 5.5 GHz, and 5.8 GHz is 3.45 dBi, 2.59 dBi, and 1.76 dBi, respectively, among which the maximum gain at 8.01 GHz is 5.23 dBi. As shown in Fig. 10, the strong current of the three frequencies is mainly distributed at the feeding point and on the transmission line.

## III. MEASUREMENTS

The proposed antenna is a combination of three technologies: CPW, back ground, and parasitic on CPW. This structure was subjected to precision machining and measurements to further validate the design. The antenna was measured using a network analyzer (CETC41, AV3629A) with a 50Ω SMA connector for back-feed at the feed point. A photo of the antenna prototype is shown in Fig. 12. The simulated return loss with a bandwidth of 3.3377 GHz (4.8337 GHz-8.1714 GHz) and measured return loss with a bandwidth of 3.38 GHz (3.95 GHz-7.33 GHz) values are shown in Fig. 13. Fig. 13 also shows that the simulated return loss is −50.8151dB at 5.25GHz and the measured return loss is −34.7348dB at 4.57GHz. Fig. 14 shows the simulation and measurement data of proposed antenna gain in the range of 5GHz to 6GHz. The measured gain range is 1.61 to 3.87dBi. The 2-D radiation pattern (E-plane and H-plane) was measured at 5.2 GHz, 5.5 GHz, 5.8 GHz, respectively in Fig. 15. As can be seen from the figure, The 2-D radiation pattern realizes circular polarization with *H-plane* of Fig. 15(a), double beam with *E-plane* of Fig. 15(a)-(c) and four directions with *H-plane* of Fig. 15(b)-(c).

## IV. CONCLUSION

The results of this study suggest that a miniaturized patch antenna with extended bandwidth can be realized after parameter optimization by ANSYS HFSS (Ver. 15). The analysis results combining return loss and ellipse slice are relevant to the design (Fig. 4), so the proposed design includes an ellipse slice. A parasitic rectangular patch was built into the CPW (Fig. 7(b)) to achieve optimal broadband effects. A prototype of the antenna was fabricated to test it by comparison against the simulated antenna; in both cases, the design achieved two-beam and four-beam performance.

The proposed broadband antenna was designed based on careful review of the literature, design optimization, guidance from an instructor, and multiple measurements. Simulation and experimental results are in accordance. The materials used to fabricate the prototype are low in cost; additionally, the antenna is small in size and has high bandwidth, low radiation, easy heat dissipation, high mechanical strength, and a simple structure which can be easily manufactured. It can be used in WLAN, RFID, and WiMAX frequency bands.

## REFERENCES

[1] G. Gui, F. Liu, J. Sun, J. Yang, Z. Zhou, and D. Zhao, "Flight delay prediction based on aviation big data and machine learning," *IEEE Trans. Veh. Technol.*, vol. 69, no. 1, pp. 140–150, Jan. 2020.
[2] J. Sun, W. Shi, Z. Yang, J. Yang, and G. Gui, "Behavioral modeling and linearization of wideband RF power amplifiers using BiLSTM networks for 5G wireless systems," *IEEE Trans. Veh. Technol.*, vol. 68, no. 11, pp. 10348–10356, Nov. 2019.
[3] P. Liu, X. Zhu, Z. H. Jiang, Y. Zhang, H. Tang, and W. Hong, "A compact single-layer Q-band tapered slot antenna array with phase-shifting inductive windows for endfire patterns," *IEEE Trans. Antennas Propag.*, vol. 67, no. 1, pp. 169–178, Jan. 2019.
[4] T. Yun, K. Jiang, H. Hou, F. An, B. Chen, A. Jiang, W. Li, and L. Xue, "Rubber tree crown segmentation and property retrieval using ground-based mobile LiDAR after natural disturbances," *Remote Sens.*, vol. 11, no. 8, p. 902, 2019.
[5] T. Yun, L. Cao, and F. An, "Simulation of multi-platform LiDAR for assessing total leaf area in tree crowns," *Agricult. Forest Meteorol.*, vols. 276–277, Oct. 2019, Art. no. 107610.

[6] X. Fang, G. Wen, D. Inserra, Y. Huang, and J. Li, "Compact wideband CPW-fed meandered-slot antenna with slotted Y-shaped central element for Wi-Fi, WiMAX, and 5G applications," *IEEE Trans. Antennas Propag.*, vol. 66, no. 12, pp. 7395–7399, Dec. 2018.
[7] Y. Yashchyshyn, K. Derzakowski, G. Bogdan, K. Godziszewski, D. Nyzovets, C. H. Kim, and B. Park, "28 GHz switched-beam antenna based on S-PIN diodes for 5G mobile communications," *IEEE Antennas Wireless Propag. Lett.*, vol. 17, no. 2, pp. 225–228, Feb. 2018.
[8] J. Zeng and K.-M. Luk, "Single-layered broadband magnetoelectric dipole antenna for new 5G application," *IEEE Antennas Wireless Propag. Lett.*, vol. 18, no. 5, pp. 911–915, May 2019.
[9] S.-W. Qu, C. Ruan, and B.-Z. Wang, "Bandwidth enhancement of wide-slot antenna fed by CPW and microstrip line," *IEEE Antennas Wireless Propag. Lett.*, vol. 5, pp. 15–17, 2006.
[10] C.-Y. Huang and C.-W. Ling, "CPW feed circularly polarised microstrip antenna using asymmetric coupling slot," *Electron. Lett.*, vol. 39, no. 23, p. 1627, Nov. 2003.
[11] C.-Y. Huang and C.-W. Ling, "CPW feed circularly polarised microstrip antenna using asymmetric coupling slot," *Electron. Lett.*, vol. 39, no. 23, p. 1627, Nov. 2003.
[12] G. Li, H. Zhai, T. Li, L. Li, and C. Liang, "CPW-fed S-shaped slot antenna for broadband circular polarization," *IEEE Antennas Wireless Propag. Lett.*, vol. 12, pp. 619–622, 2013.
[13] J.-H. Lu and Y.-Y. Lee, "Planar compact triple-band monopole antenna for IEEE 802.16 m worldwide interoperability for microwave access system," *IET Microw., Antennas Propag.*, vol. 7, no. 13, pp. 1045–1054, Oct. 2013.
[14] S.-S. Jeng, J.-M. Chen, C.-W. Tsung, and Y.-F. Lu, "Coverage probability analysis of IEEE 802.16 system with smart antenna system over Stanford University interim fading channels," *IET Commun.*, vol. 4, no. 1, pp. 91–101, 2010.
[15] U. Chakraborty, A. Kundu, S. K. Chowdhury, and A. K. Bhattacharjee, "Compact dual-band microstrip antenna for IEEE 802.11a WLAN application," *IEEE Antennas Wireless Propag. Lett.*, vol. 13, pp. 407–410, 2014.
[16] D.-O. Han, J.-H. Kim, and S.-G. Park, "A dual band CMOS receiver with hybrid down conversion mixer for IEEE 802.11a/b/g/n WLAN applications," *IEEE Microw. Wireless Compon. Lett.*, vol. 20, no. 4, pp. 235–237, Apr. 2010.
[17] C.-J. Wang and C.-H. Chen, "CPW-fed stair-shaped slot antennas with circular polarization," *IEEE Trans. Antennas Propag.*, vol. 57, no. 8, pp. 2483–2486, Aug. 2009.
[18] S.-W. Zhou, P.-H. Li, Y. Wang, W.-H. Feng, and Z.-Q. Liu, "A CPW-fed broadband circularly polarized regular-hexagonal slot antenna with L-shape monopole," *IEEE Antennas Wireless Propag. Lett.*, vol. 10, pp. 1182–1185, 2011.
[19] R. K. Saini, S. Dwari, and M. K. Mandal, "CPW-fed dual-band dual-sense circularly polarized monopole antenna," *IEEE Antennas Wireless Propag. Lett.*, vol. 16, pp. 2497–2500, 2017.
[20] H.-G. Xue, X.-X. Yang, and Z. Ma, "A novel microstrip-CPW fed planar slot antenna with broadband and circular polarization," *IEEE Antennas Wireless Propag. Lett.*, vol. 14, pp. 1392–1395, 2015.
[21] J.-Y. Chiou, J.-Y. Sze, and K.-L. Wong, "A broad-band CPW-fed strip-loaded square slot antenna," *IEEE Trans. Antennas Propag.*, vol. 51, no. 4, pp. 719–721, Apr. 2003.
[22] Z.-J. Jin and T.-Y. Yun, "Compact wideband open-end slot antenna with inherent matching," *IEEE Antennas Wireless Propag. Lett.*, vol. 13, pp. 1385–1388, 2014.
[23] J. Pourahmadazar, C. Ghobadi, J. Nourinia, N. Felegari, and H. Shirzad, "Broadband CPW-fed circularly polarized square slot antenna with inverted-L strips for UWB applications," *IEEE Antennas Wireless Propag. Lett.*, vol. 10, pp. 369–372, 2011.
[24] D. Unnikrishnan, D. Kaddour, S. Tedjini, E. Bihar, and M. Saadaoui, "CPW-fed inkjet printed UWB antenna on ABS-PC for integration in molded interconnect devices technology," *IEEE Antennas Wireless Propag. Lett.*, vol. 14, pp. 1125–1128, 2015.
[25] M. Ben Kilani, M. Nedil, N. Kandil, M. C. E. Yagoub, and T. A. Denidni, "Wideband directional elliptic coupler based on CB-CPW technology," *Electron. Lett.*, vol. 48, no. 12, pp. 710–712, 2012.
[26] A. Kunwar, A. K. Gautam, and B. K. Kanaujia, "Inverted L-slot triple-band antenna with defected ground structure for WLAN and WiMAX applications," *Int. J. Microw. Wireless Technol.*, vol. 9, no. 1, pp. 191–196, Jun. 2015.
[27] A. Kunwar and A. K. Gautam, "Fork-shaped planar antenna for bluetooth, WLAN, and WiMAX applications," *Int. J. Microw. Wireless Technol.*, vol. 9, no. 4, pp. 859–864, Jul. 2016.

**ZHENDONG DING** was born in Suzhou, Anhui, China, in May 1992. He received the B.Sc. degree from the Nanjing Normal University Zhongbei College, China, in 2015, and the M.S. degree in instrumentation engineering from Nanjing Forestry University, Nanjing, China, in 2019. His main research interests include design and optimization of photonic crystal, monopole antennas, RFID, and antennas for WLAN/WIMAX applications.

**DAN ZHANG** (Member, IEEE) received the B.S. degree in mechanical engineering from the Dalian University of Technology, Dalian, China, in 1999, and the M.S. and Ph.D. degrees in electromagnetic waves and communication engineering from Kyushu University, Fukuoka, Japan, in 2004 and 2007, respectively. In 2015, he was introduced to Nanjing Forestry University as a high-level talent. He is currently a Professor of electronic and communication engineering with the College of Information Science and Technology, Nanjing Forestry University, China. In recent years, more than 50 articles have been published by the first author, and more than ten patents have been applied for granted. He has been invited by the International Professional Society for many times to preside over international conferences or give academic speeches. His research interests include electromagnetic field theory, microwave and optical technology, and nondestructive testing and imaging. He is also an Associate Editor of *IEICE Electronics Express* and a Reviewer of several internationally renowned professional journals.

**CHUNYU MA** was born in Wuxi, China, in 1995. She received the B.S. degree in electronic information engineering from the Nanjing Forestry University of Information Science and Technology, Nanjing, China, in 2014, where she is currently pursuing the M.S. degree in electronic system. Her current interests include substrate integrated waveguide components and systems, especially the filers and terahertz antenna.